Impact of VSG Parameters on Transient Performance of Solar PV based System

Rakesh Kumar Panda, Abheejeet Mohapatra and S. C. Srivastava
Department of Electrical Engineering, Indian Institute of Technology Kanpur, India 208016
Email: rpanda@iitk.ac.in; abheem@iitk.ac.in; scs@iitk.ac.in

***Abstract*—The impact of Virtual Synchronous Generator (VSG) parameters on the transient performance of Solar Photo-Voltaic (SPV) based system has been analyzed in this paper. In addition, the variations in Kinetic Energy (KE) and Potential Energy (PE) components of a Structure Preserving Energy Function (SPEF) for the system under consideration have also been analyzed for the same purpose. In order to do this, state space model of the SPV system with VSG controller has been developed. SPEF has then been derived with this model for a SPV source connected to a Synchronous Generator (SG) by a cable with the nonlinear load. In order to analyze the transient behavior of the system under 3ϕ bolted fault and induction motor switching, a nonlinear Runge-Kutta 4^{th} order method is used for numerical simulation. Results from Real Time Digital Simulator (RTDS) show that the variations in KE and PE of SPEF can aid in assessing the transient behavior of SPV based system.**

***Index Terms*—Solar PV, Virtual Synchronous Generator, Energy Function, Transient performance.**

I. Introduction

Integration of inverter interfaced SPV sources in the conventional system has undesirable impact on system transient stability as compared to a conventional generator [1]. In a traditional generator, system transient stability is governed by the sizable rotating mass of generators. The same is not true for SPV sources. To enhance system inertia of SPV based systems for improved transient stability, control methods like VSG [2], synchronverter [3], etc. have been proposed in the literature. Of these, VSG is more popular due to its easy implementation [2].

It is thus evident that the assessment of system transient stability of SPV based system with VSG is of paramount importance. Majority of literature deal with the issue of stability [4] and inertia contribution through VSG [2] for SPV based systems. However, to the best of the authors' knowledge, no attempt has been made to analyze the impact of VSG parameters on the transient behavior of SPV source based system in the presence of system disturbance using the energy function concept. The benefit of doing so by the energy function method is that it takes less time to give solution (degree of stability) and also provides additional information to design predictive control for the system [5]. Energy function has been often used to assess the transient stability of conventional power system [5]. However, to overcome the conservativeness of its results and consideration of a simple generator model without its control circuit, Structure Preserving Energy Function (SPEF) of the system was first introduced in [6]. SPEF includes detail modeling of a generator with its control circuit and also considers models of load and transmission system. Use of SPEF for transient stability evaluation in the conventional system can be seen in [7].

978-1-5386-6159-8/18/$31.00 © 2018 IEEE

Thus, the major contributions of this paper are: first, to analyze the impact of VSG parameters on the transient performance of SPV based system in the event of disturbances with variations in SPEF. Second, the detailed state space model of SPV source with VSG is derived for this purpose. SPV source is assumed to be delivering maximum power to Point of Common Coupling (PCC), regardless of system condition. Third, the derived state space model of VSG is used to obtain SPEF for transient behavior analysis. For robust transient performance analysis under 3ϕ bolted fault and induction motor switching, a nonlinear load, which is a combination of 3ϕ Induction Motor (IM) and ZIP load, is used.

II. State Space model of SPV system

The focal point of the paper is to study the impact of VSG parameters on the transient performance of SPV based system during 3ϕ bolted fault and nonlinear load switching. Generally, a power source near the fault and load point (the SPV source with VSG in fig. 1) is modeled in detail for transient stability analysis. Hence, detailed modeling of the VSG controller based SPV source is proposed. For simplicity, SG is modeled using classical model. This section first reviews the overall system structure, which is used for transient stability analysis and, then, mathematical modeling of each component is discussed.

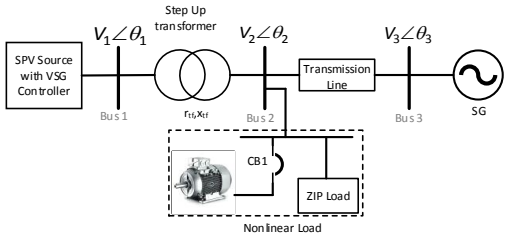

Fig. 1: Single line diagram of simulated system

A. System Overview

The single line diagram of the simulated system is shown in fig. 1. VSG based SPV source, and SG is supplying an IM and a ZIP load. IEEE type 1 governor/ turbine and IEEE type ST1 excitation system are used for SG to control active power output and terminal voltage, respectively [8]. VSG controller

works for governor and excitation system action for SPV source. The detailed control operation of VSG with associated mathematical modeling is discussed next.

B. SPV based Source with VSG Controller [2]

The implementation structure of the SPV source is shown in fig. 2. The energy storage unit is used primarily to imitate the Kinetic Energy (KE) of the SG. During a disturbance, it aids to store additional power supplied by SPV source. The inverter and its associated filter unit act as an interface between SPV source and PCC.

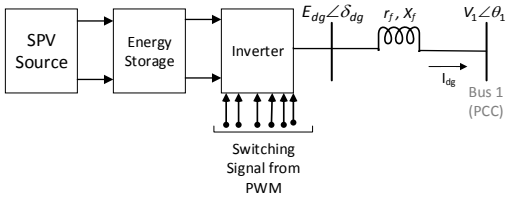

Fig. 2: Basic SPV integration with PCC

The inverter switching signal is decided by the VSG controller, which is shown in fig. 3. To mimic the SG characteristic, VSG block solves the swing equation using 4^{th} order Runga-Kutta method to decide the inverter power output. The mechanical power reference to the VSG block, P_{m_dg} is calculated by the MPPT algorithm, i.e., $P_{m\_dg} = P_{MPPT}$. The real and reactive power injected at PCC by SPV source are given by

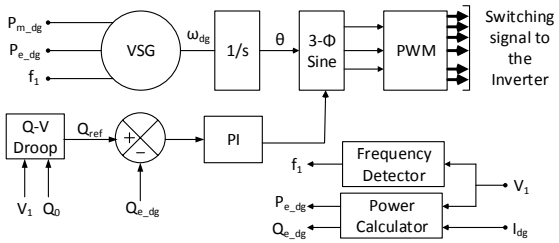

Fig. 3: Basic VSG control Structure

$$P_{e\_dg} = \frac{E_{dg}V_1}{x_{dg}}\sin(\delta_{dg} - \theta_1) \tag{1}$$

$$Q_{e\_dg} = \frac{E_{dg}^2}{x_{dg}} - \frac{E_{dg}V_1}{x_{dg}}\cos(\delta_{dg} - \theta_1) \tag{2}$$

where, E_{dg} and δ_{dg} are inverter terminal voltage and associated phase angle, respectively. V_1 and θ_1 are voltage magnitude and associated phase at PCC. The $x_{dg} = x_f$ is transfer reactance between SPV source and PCC. E_{dg} is determined by reactive power control loop, which gives $Q_{ref} = Q_0 - k_q(V_1 - V_{10})$ signal by taking V_1 as an input to the $Q - V$ drop control. Q_0 is the reactive power supplied by SPV source at nominal voltage V_{10} and k_q is the $Q - V$ droop coefficient.

C. Proposed State Space Model of VSG Controller

Dynamics of real power loop for VSG block can be written in the form of swing equation as

$$\dot{\delta}_{dg} = \omega_{dg} \tag{3}$$

$$M_{dg}\dot{\omega}_{dg} = P_{m\_dg} - P_{e\_dg} - D_{dg}(\omega_{dg} - \omega_0) \tag{4}$$

where, ω_{dg} is output frequency of VSG and ω_0 is the nominal system frequency. M_{dg} and D_{dg} are virtual inertia and damping coefficient of SPV source, respectively. On similar lines, the dynamics of reactive control loop can be derived as

$$E_{dg} = (Q_0 - k_q(V_1 - V_{10}) - Q_{e\_dg})\left(k_{p_{dg}} + \frac{k_{i_{dg}}}{s}\right) \tag{5}$$

where, $k_{p_{dg}}$ and $k_{i_{dg}}$ are the PI parameters of the reactive control loop. Since, SPV source is considered, the reactive power support is zero, i.e. $Q_0 = 0$. Dynamics of PCC voltage is ignored i.e. $\dot{V}_1 = 0$. Laplace inverse of (5) yields

$$\dot{E}_{dg} = -k_{p_{dg}}\dot{Q}_{e\_dg} - k_q k_{i_{dg}}(V_1 - V_{10}) - k_{i_{dg}}Q_{e\_dg} \tag{6}$$

From (2), $\dot{Q}_{e\_dg}$ can be written as

$$\begin{aligned}\dot{Q}_{e\_dg} = \frac{2E_{dg}}{x_{dg}}\dot{E}_{dg} - \frac{V_1\cos(\delta_{dg} - \theta_1)}{x_{dg}}\dot{E}_{dg} \\ + \frac{E_{dg}V_1\sin(\delta_{dg} - \theta_1)}{x_{dg}}\dot{\delta}_{dg}\end{aligned} \tag{7}$$

On substituting $\dot{\delta}_{dg}$ from (3) and $\dot{Q}_{e\_dg}$ from (7) in (6), the dynamics of reactive control loop can be expressed as

$$\begin{aligned}T_{dg}\dot{E}_{dg} = -k_{p_{dg}}\frac{V_1\sin(\delta_{dg}-\theta_1)}{x_{dg}}\omega_{dg} + k_{i_{dg}}\frac{V_1}{x_{dg}}\cos(\delta_{dg}-\theta_1) \\ -k_{i_{dg}}\frac{E_{dg}}{x_{dg}} - \frac{k_{i_{dg}}k_q(V_1-V_{10})}{E_{dg}}\end{aligned} \tag{8}$$

where, $T_{dg} = (1 + k_{p_{dg}}\frac{2E_{dg}}{x_{dg}} - k_{p_{dg}}\frac{V_1}{x_{dg}}\cos(\delta_{dg} - \theta_1))\frac{1}{E_{dg}}$.

D. SG Model [9]

Classical model of SG is considered for transient stability analysis. Hence, the quadrature axis voltage behind the transient reactance, $E'_{q_{sg}}$ is assumed constant and direct axis and quadrature axis reactances are considered equal, i.e. $x_{d_{sg}} = x_{q_{sg}}$. Dynamics of SG can be described by the following swing equation

$$\dot{\delta}_{sg} = \omega_{sg} \tag{9}$$

$$M_{sg}\dot{\omega}_{sg} = P_{m\_sg} - P_{e\_sg} - D_{sg}(\omega_{sg} - \omega_0) \tag{10}$$

where, M_{sg} and D_{sg} are the inertia and damping coefficient of SG, respectively. δ_{sg} is load angle of SG and ω_{sg} is SG frequency. P_{m_sg} and P_{e_sg} are the mechanical input and electrical output of SG, respectively.

E. Nonlinear Load Model [9]

The nonlinear load in fig. 1 is a combination of a static ZIP load and an IM. Hence, total real and reactive power loads are $P_L = P_{ZIP} + P_{IM}$ and $Q_L = Q_{ZIP} + Q_{IM}$, respectively. The ZIP load model can be expressed as

$$\begin{aligned}P_{ZIP} = P_0\left[a_Z\left(\frac{V_2}{V_{20}}\right)^2 + a_I\left(\frac{V_2}{V_{20}}\right) + a_P\right] = f_p(V_2) \\ Q_{ZIP} = Q_0\left[b_Z\left(\frac{V_2}{V_{20}}\right)^2 + b_I\left(\frac{V_2}{V_{20}}\right) + b_P\right] = f_q(V_2)\end{aligned} \tag{11}$$

where, a_Z, a_I, a_P are constant impedance, current and power coefficients, respectively of real power load. b_Z, b_I, b_P are

similar coefficients for reactive power load. P_0 and Q_0 are respective nominal values at nominal voltage V_{20}.

IM dynamics [10], considering both electrical and mechanical transients can be written as

$$\dot{E}^{'}_{d_{im}}=\frac{1}{T^{'}_{0_{im}}}[E^{'}_{d_{im}}+(X_{im}-X^{'}_{im})I_{q_{im}}]+(\omega_{r_{im}}-\omega_0)E^{'}_{q_{im}} \quad (12a)$$

$$\dot{E}^{'}_{q_{im}}=\frac{1}{T^{'}_{0_{im}}}[E^{'}_{q_{im}}+(X_{im}-X^{'}_{im})I_{d_{im}}]-(\omega_{r_{im}}-\omega_0)E^{'}_{d_{im}} \quad (12b)$$

$$\dot{\omega}_{r_{im}}=\frac{\omega_0}{2H_{im}}(T_{e\_im}-T_{m\_im}) \quad (12c)$$

The standard notations defined in [10] are used in (12). The real and reactive powers consumed by the IM can be expressed as $P_{IM} = 1.5\,(V_{d2}I_{d_{im}} + V_{q2}I_{q_{im}})$ and $Q_{IM} = 1.5\,(V_{q2}I_{d_{im}} - V_{d2}I_{q_{im}})$.

F. Transmission Line and Transformer Model

The transmission line is modeled using lumped parameter π representation and the transformer is replaced by its leakage impedance i.e $z_{tf} = r_{tf}+jx_{tf}$. Real and reactive power flows in a line between bus i and bus j are

$$\begin{aligned} P_{ij} &= V_iV_j(G_{ij}\cos\theta_{ij} + B_{ij}\sin\theta_{ij}) \\ Q_{ij} &= V_iV_j(G_{ij}\sin\theta_{ij} - B_{ij}\cos\theta_{ij}) \end{aligned} \quad (13)$$

where, G_{ij} and B_{ij} are real and imaginary parts of $(i,j)^{th}$ element of system admittance matrix. $\theta_{ij} = \theta_i - \theta_j$ and V_i and V_j are the i^{th} and j^{th} bus voltage magnitudes, respectively.

III. Structure Preserving Energy Function [9]

The objective of this section is to derive a SPEF for the impact of VSG parameters on transient stability analysis of the system in fig. 1. The assumptions, considered for derivation of the energy function, are *a*) SG is replaced by classical model, *b*) governor of SG does not respond during fault period, *c*) for SPV source, insolation and temperature remains unchanged during the transient period, *d*) post-fault and pre-fault operating points are same. The derived SPEF includes the load dynamics, the effect of VSG controller as well as network dynamics. The energy function defined for the system in fig. 1 is

$$W_{Tot}(\delta,\omega,E,V,\theta,t) = W_{KE_T} + W_{PE_T} \quad (14)$$

where, W_{Tot} is the total energy of the system and W_{KE_T}, W_{PE_T} are the total KE and total Potential Energy (PE), respectively.

A. Total Kinetic Energy W_{KE_T}

Usually, KE is associated with the rotating mass of the machine. System in fig. 1 has two rotational masses i.e. SG and IM. However, to improve the KE of the system, VSG controller is used for SPV source, which introduces virtual KE into the system. Therefore, W_{KE_T} can be written as

$$W_{KE_T}(\omega) = W_{KE\_sg} + W_{KE\_dg} + W_{KE\_im} \quad (15)$$

where, W_{KE_sg} = KE associated with SG = $\frac{1}{2}M_{sg}\omega^2_{sg}$, W_{KE_dg} = KE associated with DG = $\frac{1}{2}M_{dg}\omega^2_{dg}$ and W_{KE_im} = KE associated with IM = $\frac{1}{2}M_{im}\omega^2_{im}S$. Value of W_{KE_sg} can be obtained by integrating left hand side of (10), after multiplying with $\dot{\delta}_{sg}$. By adopting similar procedure to (4) and (12c), corresponding values of W_{KE_dg} and W_{KE_im} can be obtained. $S = 1$, when CB1 is closed in fig. 1 and $S = 0$, when CB1 is opened. Energy associated with damping is not considered here as it is not significant and appropriate justification of not considering this is given in [11].

B. Total Potential Energy, W_{PE_T}

PE of a system is sum of integrals of the accelerating power associated with the power sources and sum of energy associated with network element. PE of the SPV source, SG and IM can be obtained by integrating right hand sides of the (4), (10) and (12c), respectively. By integrating (11) and (13), PE of nonlinear load and transmission network can be obtained. More details can be seen in [9]. The total PE, W_{PE_T} can be written as

$$\begin{aligned} W_{PE_T}(\delta,E,V,\theta,t) =& W_{PE\_sg} + W_{PE\_dg} + W_{PE\_im} \\ &+ W_{PE\_ZIP} + W_{PE\_tl} \end{aligned} \quad (16)$$

The PE associated with SG, i.e. W_{PE_sg} can be stated as

$$W_{PE\_sg} = W_{PE\_sg_1}(\delta) + W_{PE\_sg_2}(\delta,E,V,\theta) \quad (17)$$

where, $W_{PE\_sg_1}$ = PE due to $P_{m\_sg} = -P_{m\_sg}(\delta_{sg} - \delta_{sg0})$ and $W_{PE\_sg_2}$ = PE due to x_{sg}. Appropriate expression of $W_{PE\_sg_2}$ can be seen in [9]. The PE associated with DG, i.e. W_{PE_dg} can be expressed as

$$W_{PE\_dg} = W_{PE\_dg_1}(\delta) + W_{PE\_dg_2}(\delta,E,V,\theta) + W_{PE\_dg_3}(E) \quad (18)$$

where,

$$W_{PE\_dg_1} = \text{PE due to } P_{m\_dg} = -P_{m\_dg}(\delta_{dg} - \delta_{dg0}) \quad (19a)$$

$$\begin{aligned} W_{PE\_dg_2} =& \text{PE due to } x_{dg} \\ =& \frac{1}{2x_{dg}}\big[(E^2_{dg} + V_1^2 - 2E_{dg}V_1\cos(\delta_{dg} - \theta_1)) \\ &-(E^2_{dg0} + V_{10}^2 - 2E_{dg0}V_{10}\cos(\delta_{dg0} - \theta_{10}))\big] \end{aligned} \quad (19b)$$

$$\begin{aligned} W_{PE\_dg_3} =& \text{PE due to } E_{dg} \\ =& \big[-k_{p_{dg}}k_{s1}\sin(\delta_{dg} - \theta_1)\omega_{dg} + k_{i_{dg}}k_{s1}\cos(\delta_{dg} - \theta_1) - \\ & k_{s2}E^2_{dg} + k_{s3}\ln(E_{dg})\big] - \big[-k_{p_{dg}}k_{s10}\sin(\delta_{dg0} - \theta_{10})\omega_{dg} \\ & + k_{i_{dg}}k_{s1}\cos(\delta_{dg} - \theta_1) - k_{s2}E^2_{dg} + k_{s3}\ln(E_{dg0})\big] \end{aligned} \quad (19c)$$

and $k_{s1} = \frac{V_1E_{dg}}{x_{dg}}$, $k_{s2} = \frac{k_{i_{dg}}}{x_{dg}}$, $k_{s3} = k_{i_{dg}}k_q(V_1 - V_{10})$, $k_{s10} = \frac{V_{10}E_{dg0}}{x_{dg}}$. The PE associated with ZIP load, i.e. W_{PE_ZIP} is

$$W_{PE\_ZIP} = W_{PE\_ZIP_P}(t) + W_{PE\_ZIP_Q}(V) \quad (20)$$

where, $W_{PE\_ZIP_P}$ = PE due to$P_{ZIP} = \int_{t_0}^{t} f_p(V_2)\left(\frac{\mathrm{d}\theta_2}{\mathrm{d}t}\right)\mathrm{d}t$ and $W_{PE\_ZIP_Q}$ = PE due to$Q_{ZIP} = \int_{V_{20}}^{V_2} f_q(V_2)\left(\frac{\mathrm{d}V_2}{V_2}\right)$.

On similar lines, PE due to IM [11] can be written as

$$W_{PE\_IM} = \left(T_{m\_im}\delta_{im} + \frac{1}{2}X_{im}I_{d_{im}} + \frac{1}{2}X^{'}_{im}I_{q_{im}}\right)\Bigg|^{\delta_{im}I_{d_{im}}I_{q_{im}}}_{\delta_{im0}I_{d_{im0}}I_{q_{im0}}} \quad (21)$$

while the same for transmission line and transformer are

$$W_{PE\_tl} = W_{PE\_tl_B} + W_{PE\_tl_G} \quad (22)$$

where,

$W_{PE\_tl_B}$=PE due to B_{ij}

$$=-\frac{1}{2}\sum_{i=1}^{n}\sum_{j=1}^{n}B_{ij}(V_iV_j\cos\theta_{ij}-V_{i0}V_{j0}\cos\theta_{ij0})$$

$W_{PE\_tl_G}$=PE due to G_{ij}(Path dependent)

$$=\sum_{i=1}^{n}\sum_{j=1}^{n}G_{ij}\int V_iV_j\sin\theta_{ij}\mathrm{d}(\theta_i+\theta_j)$$

C. Significance of Variations in SPEF

It can be seen from (15), (18) and (19c) that VSG parameters, i.e. virtual inertia M_{dg}, reactive power loop parameters $k_{i_{dg}}$ and $k_{p_{dg}}$ (and virtual active power damping coefficient D_{dg} when considered) have direct impact on KE and PE functions. Conventionally, the impact of the control circuit parameters of a generator has not been considered in the energy function evaluations [9]. However, here, this has been considered and is one of the contributions of this paper. Also, it is to be noted that the transient behavior of a system during a disturbance can be analyzed by observing variations in the system states'. However, the reliability of such an analysis depends on which state is being observed. On the other hand, variation in the total KE and/ or PE of a system during a disturbance can directly aid in analyzing the system's transient behavior as a large variation in KE and PE implies the system is prone to instability if the disturbance is allowed to persist. Also, if the time taken for KE or PE to settle at post-disturbance value is large, then it indicates that the system has less damping. SPEF thus provides an accurate energy profile considering the effect of all system components along with the control parameters of VSG.

IV. Simulation Results

System data for the considered system in fig. 1 is given in table I. A $1km$ long, $70mm^2$ three core XLPE insulated cable is used as the transmission line (associated parameters are in [12]). At steady state, SPV power output at PCC is $375kW$. SG accounts for the mismatch power. For SPEF evaluations, bus voltage phasors obtained by simulating the system in RTDS. The measured bus voltages for a specific test scenario are used in numerical simulations. Runge-Kutta 4^{th} order method is used to solve the differential equations for numerical simulation. To obtain the initial conditions, Newton-Raphson power flow is solved. The transient behavior of the system is analyzed under the following conditions.

A. Case 1: 3ϕ Bolted Fault

A 3ϕ bolted fault at bus 1 is simulated at $2s$ for 2 cycles, i.e. $40ms$. Also, as can be seen from (15), M_{dg} has the direct impact on system's KE, and, hence, the effect of any change in KE is quite straightforward (higher is M_{dg}, large is system's KE and thus improved system inertia) and has not been discussed further. What is rather interesting to see is the effect of change in $k_{i_{dg}}$, $k_{p_{dg}}$ and D_{dg} on SPEF. Table II

TABLE I: Data for System in fig. 1

SG			
Parameter	Values	Parameter	Values
V_{b_sg}	$6.6kV$	S_{b_sg}	$1MVA$
P_{0_sg}	$1.0pu$	ω_0	$314.159rad/s$
H_{sg}	$2.775s$	X_d	$1.90pu$
$X_d^{'}$	$0.314pu$	$X_d^{''}$	$0.280pu$
$X_q = X_q^{'}$	$0.770pu$	$X_q^{''}$	$0.375pu$
$T_d^{''}$	$0.0348s$	$T_q^{''}$	$0.0.0346s$
SPV		**Filter details**	
E_{dg}	$0.415kV$	r_f	0.005Ω
P_{MPPT}	$0.375MW$	L_f	$0.4mH$
J_0	$56.3kgm^2$	C_f	$300\mu F$
D_0	$17pu$	**Transformer**	
θ_{pcc}	0	Turns	$415V/6.6kV$
V_{b_pcc}	$6.6kV$	x_{tf}	$0.1pu$
DC side		**Load**	
V_{DC}	$0.85kV$	P_0	$0.4MW$
C_{DC}	$5mF$	Q_0	$0.2MVAR$

TABLE II: Test Conditions

Scenario	D_{dg}(pu)	$k_{i_{dg}}$	$k_{p_{dg}}$
S1	0.17	20	0.025
	1.7		
	17		
S2	17	10	0.025
		20	
		50	
S3	17	20	0.05
			0.025
			0.0025

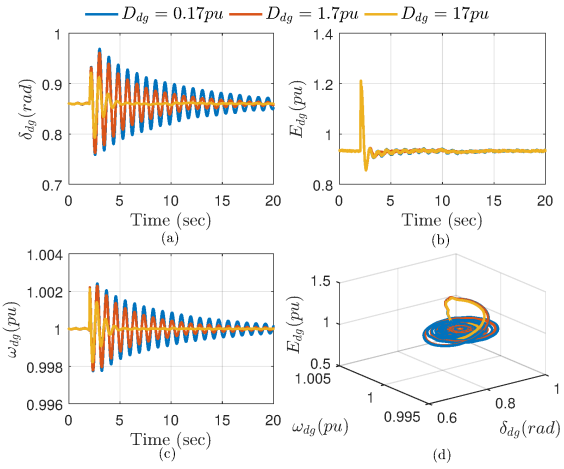

Fig. 4: SPV states in Case 1 (**S1**) (a) δ_{dg} (b) E_{dg} (c) ω_{dg} (d) state plane

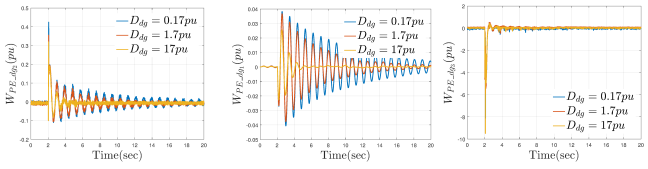

(a) PE due to electrical power (b) PE due to mechanical power (c) PE due to E_{dg}

Fig. 5: PE of VSG based SPV in Case 1 (**S1**)

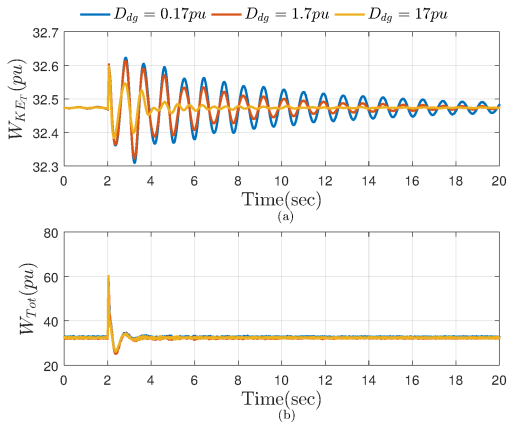

Fig. 6: (a) Total KE (b) Total energy of system in Case 1 (**S1**)

shows the various test scenarios in which the system's transient behavior is analyzed.

D_{dg} has not been explicitly considered in SPEF. However, it has direct impact on damping out the virtual rotor angle oscillation δ_{dg}, which improves the transient stability boundary [13]. To observe the impact of D_{dg}, system is tested in **S1** for the stated 3ϕ bolted fault. Associated variations are shown in Figs. 4-6. As D_{dg} increases, the states of VSG based SPV reach the pre-fault operating point quickly after the 3ϕ fault as in fig. 4. Fig. 5 shows that the oscillation in PE is higher for lower values of D_{dg}. Fig. 6 shows that KE oscillations die out quickly as D_{dg} increases.

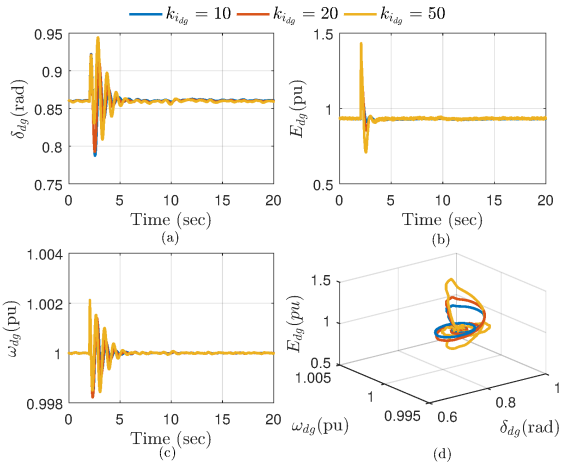

Fig. 7: SPV states in Case 1 (**S2**). (a) δ_{dg} (b) E_{dg} (c) ω_{dg} (d) state plane

Any change in $k_{i_{dg}}$ and $k_{p_{dg}}$ affects the virtual inverter terminal voltage E_{dg}, which in a way affects the VSG states. In **S2**, by decreasing $k_{i_{dg}}$ while keeping $k_{p_{dg}}$ constant, VSG based SPV states achieve their corresponding steady state operating values quickly as shown in fig. 7. The associated KE and total energy variations due to different $k_{i_{dg}}$ values are shown in fig. 8.

In **S3**, an increase in $k_{p_{dg}}$ leads to slower variation in VSG based SPV states with more settling time to reach the pre-fault operating values as shown in fig. 9. Associated variation in PE due to different $k_{p_{dg}}$ values are shown in fig. 10. A similar inference can be drawn about PE for different $k_{p_{dg}}$ values.

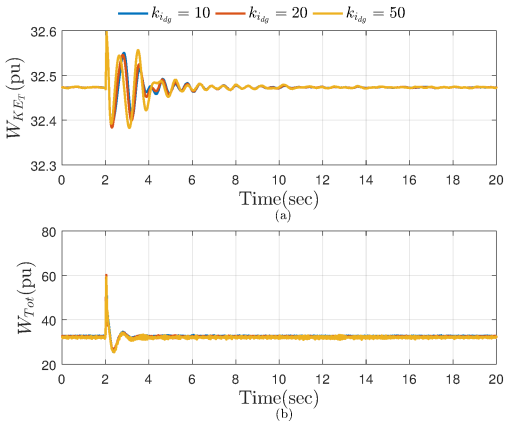

Fig. 8: (a) Total KE (b) Total energy of system in Case 1 (**S2**)

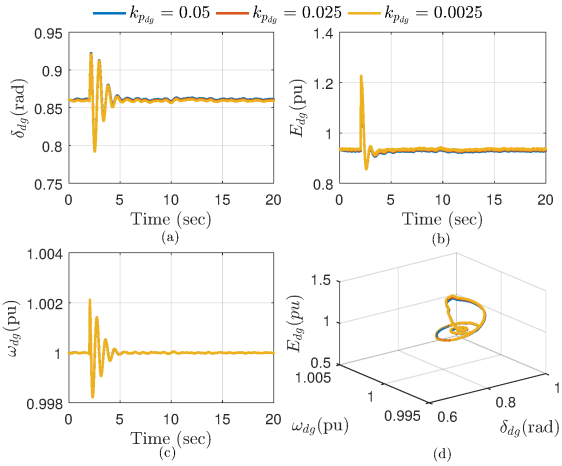

Fig. 9: SPV states in Case 1 (**S3**). (a) δ_{dg} (b) E_{dg} (c) ω_{dg} (d) state plane

B. Case 2: Induction Motor Switching

The event of IM switching has been studied for all scenarios in table II. However, due to limitation of space, **S1** with $D_{dg} = 17pu$ has been discussed here. Initially, CB1 in fig. 1 is OFF. SPV and SG feed power to ZIP load in steady state. At $2s$, 3ϕ IM (parameters in [14]) is switched ON by closing CB1. IM operates in lock free mode. Due to IM switching, a large transient is experienced in the system. Pre-equilibrium point of the VSG states, i.e. δ_{dg} and E_{dg} change due to IM switching. However, the power injected to PCC remains unchanged by SPV source. This is because the system voltage level decreases, and hence VSG adjusts its states, and thus, operates at new equilibrium point, which is shown in fig. 11a.

Similarly, to balance the real power, SG provides the

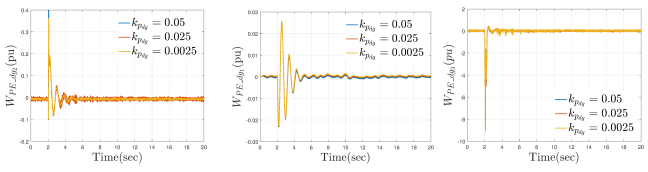

(a) PE due to Electrical Power (b) PE due to Mechanical Power (c) PE due to E_{dg}

Fig. 10: PE of VSG based SPV in Case 1 (**S3**)

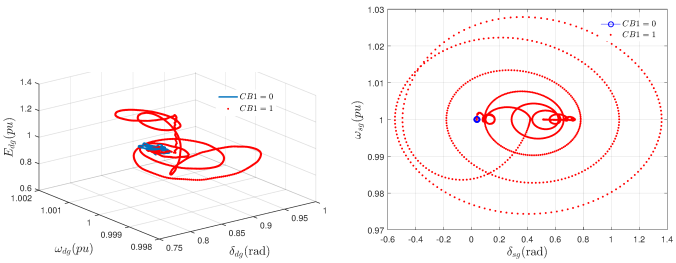

(a) State plane of VSG based SPV

(b) State plane of SG

Fig. 11: State plane of sources in Case 2

mismatch power. Therefore, the SG states i.e. δ_{sg} and ω_{sg} also change, which after oscillations settle at new steady state values as in fig. 11b. The associated variations in PE and KE during IM switching are shown in figs. 12-13. It has been observed from these variations that a higher D_{dg} with lower $k_{i_{dg}}$ and $k_{p_{dg}}$ parameters in VSG lead to improved transient behavior.

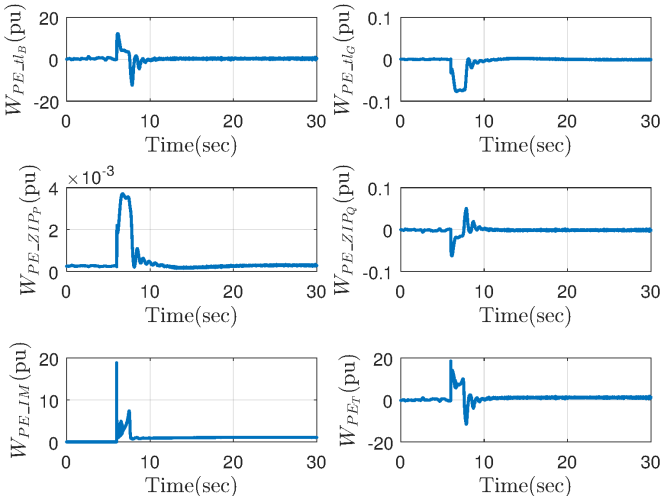

Fig. 12: PE in Case 2

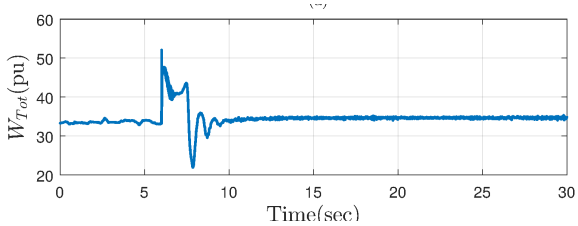

Fig. 13: Total KE in Case 2

V. Conclusion

In this paper, the impact of the change in VSG parameters on transient stability of an SPV based system has been analyzed through the novel use of a SPEF. To this end, a state space model of the SPV source with VSG controller is derived. Using the derived model, an energy candidate function in SPEF is developed considering the VSG control parameters. By including the energy function of the VSG controller with the energy function of other system components, the energy profile of the overall system is analyzed. The major advantage of this analysis is that it includes the control parameters of the VSG controller, which further helps to study the proper energy profile of the system during the transient period in the event of a disturbance. Simulation results from RTDS suggest that by choosing adequate control parameters of the VSG controller, stability of the system can be enhanced. During IM switching, reactive power consumption leads to change in the stable operating point of SPV source DG with the power injection of SPV source to PCC remaining unchanged. The proper energy profile obtained from the analysis may further aid in finding accurate stability margin and critical clearing time of the system in the event of a disturbance.

Acknowledgement

The authors would like to thank the DST/Indo-US Science and Technology Forum (IUSSTF), New Delhi, India for providing financial support to carry out this research work under an Indo-US collaborative project UI-ASSIST with project no. IUSSTF/EE/2017282B.

References

[1] R. Lasseter, A. Akhil, C. Marnay, J. Stephens, J. Dagle, R. Guttromson, A. S. Meliopoulous, R. Yinger, and J. Eto, "Integration of distributed energy resources. the CERTS microgrid concept," 2002.

[2] J. Liu, Y. Miura, and T. Ise, "Comparison of dynamic characteristics between virtual synchronous generator and droop control in inverter-based distributed generators," *IEEE Trans. Power Electron.*, vol. 31, no. 5, pp. 3600–3611, 2016.

[3] Z. Shuai, W. Huang, C. Shen, J. Ge, and Z. J. Shen, "Characteristics and restraining method of fast transient inrush fault currents in synchronverters," *IEEE Trans. Ind. Electron.*, vol. 64, no. 9, pp. 7487–7497, 2017.

[4] L. Xiong, F. Zhuo, F. Wang, X. Liu, Y. Chen, M. Zhu, and H. Yi, "Static synchronous generator model: A new perspective to investigate dynamic characteristics and stability issues of grid-tied PWM inverter," *IEEE Trans. Power Electron.*, vol. 31, no. 9, pp. 6264–6280, 2016.

[5] H.-D. Chang, C.-C. Chu, and G. Cauley, "Direct stability analysis of electric power systems using energy functions: theory, applications, and perspective," *Proceedings of the IEEE*, vol. 83, no. 11, pp. 1497–1529, 1995.

[6] A. R. Bergen and D. J. Hill, "A structure preserving model for power system stability analysis," *IEEE Trans. Power Apparatus and Syst.*, no. 1, pp. 25–35, 1981.

[7] Y.-H. Moon, B.-H. Cho, Y.-H. Lee, and H.-S. Hong, "Energy conservation law and its application for the direct energy method of power system stability," in *Power Engineering Society 1999 Winter Meeting, IEEE*, vol. 1. IEEE, 1999, pp. 695–700.

[8] P. Kundur, N. J. Balu, and M. G. Lauby, *Power system stability and control*. McGraw-hill New York, 1994, vol. 7.

[9] K. Padiyar, *Structure preserving energy functions in power systems: theory and applications*. CRC Press, 2016.

[10] V. Vignesh, S. Chakrabarti, and S. C. Srivastava, "Power system load modelling under large and small disturbances using phasor measurement units data," *IET Gener. Transm. Distrib.*, vol. 9, no. 12, pp. 1316–1323, 2015.

[11] Y. Min and L. Chen, "A transient energy function for power systems including the induction motor model," *Science in China Series E: Technological Sciences*, vol. 50, no. 5, pp. 575–584, Oct 2007.

[12] [Online]. Available: http://www.havells.com/content/dam/havells-/brouchers/Industrial Cable/Cable%20Catalogue-2016.pdf

[13] H.-D. Chiang, *Direct methods for stability analysis of electric power systems: theoretical foundation, BCU methodologies, and applications*. John Wiley & Sons, 2011.

[14] [Online]. Available: https://www.ijert.org/download/2020/an-off-line-technique-for-prediction-of-performance-characteristics-of-three-phase-induction-motor.